# A study of turbulent boundary-layer separation and reattachment

## By A. E. PERRY and B. D. FAIRLIE†

Department of Mechanical Engineering, University of Melbourne,
Parkville, Australia

An experimental and theoretical study is made of a suddenly separating and reattaching two-dimensional turbulent boundary layer on a flat surface. A separation bubble is formed on the floor of a wide parallel-sided wind-tunnel duct with the pressure field causing the bubble formation produced by fixing the shape of the flexible roof of the duct. Boundary layers on the roof are controlled and remain attached. It is found that a very satisfactory model for the flow is an inviscid one.

The boundary layer on the floor of the duct is represented by a region of constant vorticity with slip at the boundary, and it is assumed that the separation process is dominated by the interaction between this 'vortical' region and the irrotational field between the vortical region and the roof (of prescribed shape). The interface between the rotational and irrotational regions is a free boundary and may be located when all necessary boundary conditions are given. These conditions include two characteristic parameters for the adverse-pressure-gradient turbulent boundary layer which is developing upstream of the region of interest.

The problem is solved by an electrical analog method. The theoretical size and shape of the bubble and positions of separation and reattachment are in agreement with observations. The advantage of the model over most previous attempts to predict separation is that the governing equations are elliptic rather than parabolic or hyperbolic and therefore the interaction between the boundary-layer flow and the irrotational free stream is included in the calculations.

## 1. Introduction

Calculation methods for turbulent boundary layers are invariably based on the classical approach. That is, the boundary-layer approximations together with some closure hypothesis are used in conjunction with a prescribed surface pressure distribution. Some of these methods have been surprisingly successful in predicting the flow near the separation point. However, it has been felt by many authorities (e.g. see Kline *et al.* 1968) that these methods must break down in the region close to and beyond separation for the following reasons. First, the use of the boundary-layer equations destroys the elliptic nature of the Navier-

† Present address: Aeronautical Research Laboratories, Fisherman's Bend, Victoria, Australia.
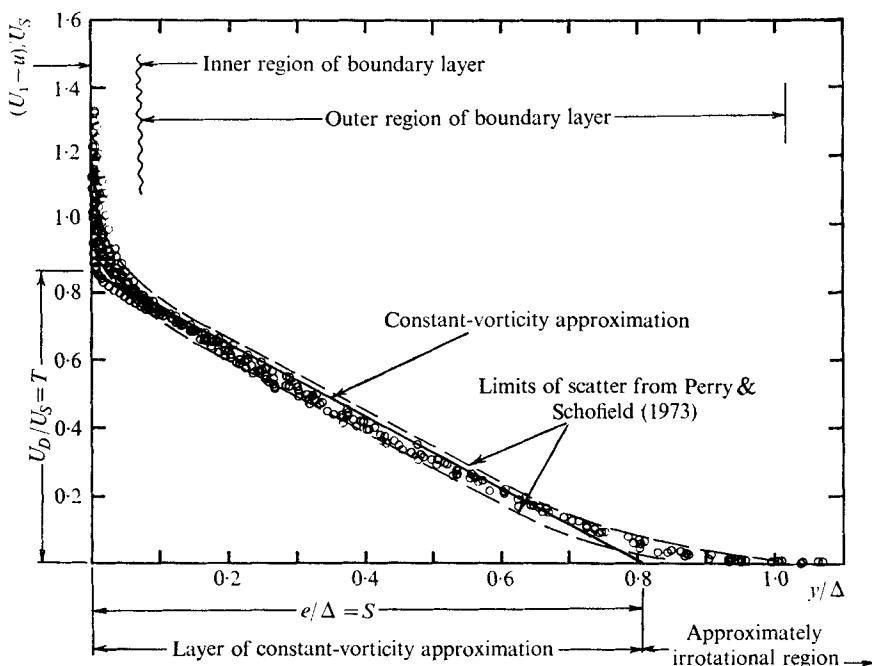
FIGURE 1. Mean-velocity profiles plotted on defect-law axes of Perry & Schofield (1973).
———, constant-vorticity approximation.

Stokes equations, thus excluding any interaction between the boundary layer and the irrotational free stream. In the separation region, the boundary-layer approximations break down and the usual step-by-step calculation procedure (valid for the parabolic or hyperbolic boundary-layer equations) must be replaced by one which takes into account all boundary conditions, both upstream and downstream. Second, the interaction between the boundary layer and the free stream precludes the prescription of the surface pressure distribution *a priori* in the region close to and beyond the separation point. Thus the classical approach appears to be inadequate for calculating the flow in regions of separation.

The authors have therefore attempted to develop a model for turbulent boundary-layer separation and reattachment for the region where the boundary-layer approximations are invalid and where the surface pressure distribution is not known *a priori*. The case considered here is that in which an adverse-pressure-gradient boundary layer is forced suddenly to separate and then reattach. To provide reliable data against which this model could be tested, an experimental programme was carried out concurrently.

The model adopted here is similar to that suggested by Kuchemann (1967) and Smith (1970) (for the trailing edge of an aerofoil) and Taulbee & Robertson (1972) (for flow upstream of a forward-facing step). The authors propose that the turbulent layer may be represented by an inviscid rotational region of constant vorticity with slip at the wall. Some confirmation of this representation is provided by the work of Perry & Schofield (1973). They calculated Reynolds-stress gradients for all the adverse-pressure-gradient layers examined at the
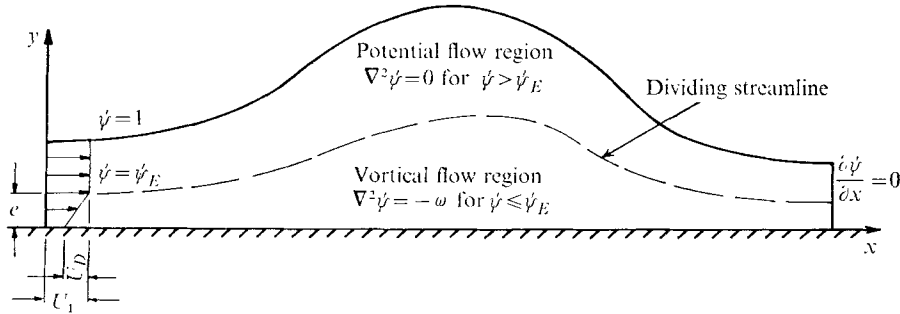
FIGURE 2. Summary of boundary conditions.

Stanford Prediction Conference (Kline *et al.* 1968; Coles & Hirst 1968) and found that, in the latter stages of development, pressure-gradient and inertia forces were dominant in the outer 80 % of the layers. Shear-stress gradients were almost two orders smaller. Thus an inviscid rotational model would appear to be plausible, particularly when the separation or reattachment occurs suddenly and is well defined. Perry & Schofield also found that such adverse-pressure-gradient layers have linear velocity distributions prior to separation, providing justification for the constant-vorticity approximation. This is illustrated in figure 1, the notation for which is explained later (§ 3.3). For the inner region of the boundary layer (also indicated in figure 1), where gradients of shear stress become significant, various approximations have been used in the past. For example, Stratford (1959) and Townsend (1960) used an inviscid rotational representation for the outer region of the layer and attempted, with some success, to match it to various forms of inner-layer representation. The approach of the present authors is to replace the inner region of the boundary layer by a vortex sheet (i.e. slip at the boundary), assuming the effect of the inner flow on the separation process to be dominated by the interaction of the rotational outer flow in the boundary layer with the irrotational external stream.

## 2. Details of model

As a first approximation, the thickening of the vortical region due to entrainment will be neglected. Therefore the proposed separation model is governed by the two-dimensional inviscid Helmholtz equation

$$D(\nabla^2\psi)/Dt = 0, \tag{1}$$

where $\psi$ is the stream function. The flow will be divided into two regions (see figure 2).

(I) An irrotational external stream, where for steady flow (1) reduces to Laplace's equation

$$\nabla^2\psi = 0. \tag{2}$$

(II) A vortical layer in which the vorticity is constant throughout with finite slip at the wall. This region separates region I from the wall. It is the rotational part of the flow, including the whole boundary layer and (when there is one) the

separation bubble and the separated shear layer bounding it. In the steady state, (1) will reduce to Poisson's equation

$$\nabla^2 \psi = f(\psi) = -\omega, \tag{3}$$

where $\omega$ is the value of the (constant) vorticity of the approaching upstream boundary layer.

It should be noted that the governing equations are elliptic in nature, requiring the specification of all boundary conditions. The interface between regions I and II must be a streamline satisfying (1) and the velocity across it must be continuous.

## 3. Boundary conditions

### 3.1. *Upstream boundary conditions*

These boundary conditions are concerned with the initial velocity profile of the layer and its thickness. Various velocity-profile models are available, e.g. see Coles (1956) or Sandborn (1959). The present work uses a defect distribution based on the similarity proposal of Perry & Schofield (1973) because of its simplicity and convenience: it requires the least possible number of parameters to specify the profile shape. This proposal has been found to represent successfully all adverse-pressure-gradient velocity profiles in layers approaching separation for which the maximum shear stress is larger than about 1·5 times the wall shear stress at a given station. Let $u$ be the $x$ component of velocity at a distance $y$ from the wall and let $U_1$ be the velocity just outside the boundary layer. A velocity scale $U_s$ and a length scale $\Delta$ can be found which collapse the data in the defect form shown in figure 1. In fact, this is how the scales $U_s$ and $\Delta$ are defined. It will be shown later that $U_s$ and $\Delta$ can be calculated from extremely simple relations once the displacement thickness $\delta^*$ and the form factor $H$ ($= \delta^*/\theta$) are known. Here $\theta$ is the momentum thickness. These latter quantities can be determined from experiment or may be predicted by any suitable calculation scheme valid for the region upstream of the separation zone. In figure 1, $T$ and $S$ are universal constants associated with the straight-line approximation shown. $U_D$ is the extrapolated velocity defect at the wall and $e$ is the value of $y$ which corresponds to the outer edge of the vortical layer, i.e. the layer of constant vorticity to be used as an approximation to the actual boundary layer at this upstream position.

Here the boundary-layer approximations are assumed to remain valid and hence as far as the electrical analog method (§ 4) is concerned the flow remains essentially parallel to the floor at this upstream station. Introduction of a small divergence at this position was found to have a very small influence on the calculated streamline pattern downstream. The distribution of the dimensionless stream function through the vortical layer upstream is then given by

$$\psi = \Omega Y^2 + \frac{U_1 - U_D}{U_0} Y, \quad 0 < Y < E, \tag{4}$$

where $E = e/L$ and $Y = y/L$. Also

$$\psi = \int_0^Y \frac{u}{U_0} dY, \quad \Omega = \frac{\omega L}{2U_0}. \tag{5}, (6)$$

$U_0$ is an upstream reference velocity and $L$ is an arbitrary length scale to be defined in § 3.3.

The distribution of the stream function in the free stream then becomes

$$\psi = \frac{U_1}{U_0} Y + \Omega E^2 - \frac{U_D}{U_0} E, \quad Y > E. \tag{7}$$

At this upstream station the free-stream velocity is taken to be $U_1$ and is invariant with $y$.

If $U_s$ and $\Delta$ are known, then $E$, $\Omega$ and $U_D$ may be found from

$$E = \frac{S\Delta}{L}, \quad U_D = TU_s, \quad \Omega = \frac{U_D}{2EU_0} = \frac{TU_sL}{2S\Delta U_0}, \tag{8}$$

where $T$ and $S$ are the universal constants defined in figure 1. It remains to determine $T$ and $S$ such that the constant-vorticity approximation matches the experimental data. The matching conditions were chosen such that the approximate and experimental velocity profiles have the same displacement thickness and that the value $\psi_E$ of the stream function at the edge of the vortical layer ($Y = E$) is the same in both cases. The appropriate values were found to be $S = 0\cdot805$ and $T = 0\cdot868$.

From the proposal of Perry & Schofield (1973) equations similar to those of Clauser (1956)† may be derived (ignoring the thin logarithmic region close to the boundary). These are

$$H = (1 - G\xi)^{-1}, \quad \Delta = \delta^*/N\xi. \tag{9},(10)$$

Here $\xi = U_s/U_1$ and $G$ and $N$ are universal constants with values $0\cdot58$ and $2\cdot86$ respectively. Thus given $\delta^*$ and $H$ from experiment, $\Delta$ and $U_s$ are known and hence the constants in (4) and (7) can be evaluated.

### 3.2. *Downstream boundary conditions*

Since vorticity is conserved along streamlines it follows that the distribution of $\psi$ downstream can be found from a knowledge of the upstream boundary conditions and the continuity equation. In the present case it is assumed that the downstream boundary is located such that the flow is once again parallel, i.e. $\partial\psi/\partial x = 0$. In fact the experiment was deliberately arranged to achieve closely this condition.

### 3.3. *Other boundary conditions*

All the boundary conditions are shown in figure 2. The upper boundary corresponds to the roof (the upper boundary layers being thin) and $\psi$ is arbitrarily taken to be unity there, thus fixing the value of $L$ in (4).

In the separated region, streamlines are closed and therefore do not originate from upstream. Therefore the vorticity there may differ from the constant

---

† The only differences from the Clauser relations are that $U_s$ is not directly related to the wall shear velocity and the above equations appear to be valid for both equilibrium and non-equilibrium layers.

value $\omega$. There is very little theoretical or experimental guidance as to the appropriate value. Taulbee & Robertson (1972) considered a varying-vorticity model and assumed a vorticity excess in the separated region upstream of their step. The work of Batchelor (1956) suggests that, at least for closed laminar separation bubbles, the vorticity should be constant within the bubble, its value being determined by the boundary conditions. The present experiment indicates a deficiency of vorticity here but in the model the vorticity is assumed to have the same constant value $\omega$ as in the rest of the vortical region. It is conjectured that the resulting solution is insensitive to the value of the vorticity close to the centre of the bubble, since by Stokes' theorem the contribution to the circulation about the closed streamline $\psi = 0$ is weighted more heavily by the vorticity in the peripheral regions of the bubble.

## 4. Method of solution of governing equations

The complexity of the problem precludes an analytic solution. Numerical solutions are possible in principle (e.g. Smith 1970). However, here an electrical analog technique employing the familiar resistance-paper method was used. The solution of Laplace's equation using steady currents is well known. However, the solution of Poisson's equation requires distributed capacitance and so a.c. voltages are applied as described by Swannell (1963) and Fairlie (1973). The physical circuit is shown in figure 3. The areas of distributed capacitance are provided by applying conducting paint to a sheet of acetate bonded to the back of the resistance paper. The solution of the governing equations then proceeds as follows. The upper and lower boundaries are defined by painting the surface of the resistance paper with conducting paint. The upstream and downstream boundaries are defined by the edges of the resistance paper, which must be cut suitably. Streamlines will be normal to these edges. The solution to Laplace's equation throughout the region is then obtained by applying an a.c. voltage between the upper and lower boundaries and tracing lines of constant a.c. voltage (streamlines) with a copper probe and voltmeter. The Laplace streamline passing through the (known) upper limit of the vortical region at the upstream boundary is then taken as a first approximation to the limit of the vortical region (the dividing streamline) and the area between this streamline and the lower boundary is provided with distributed capacitance by the application of conducting paint to the acetate backing sheet.

The voltages $V$ and $\phi$ (see figure 3) are applied and adjusted to obtain the correct external boundary conditions. A second approximation to the dividing streamline is obtained by tracing the new streamline beginning at the upstream upper limit of the vortical region and the area of distributed capacitance is then modified accordingly. This process is then repeated until two successive approximations to the dividing streamline coincide. This iterative process has been found to converge surprisingly quickly in practice (2–3 iterations for rough calculations or 7–10 iterations for greater accuracy) and in most cases monotonically. The complete streamline pattern may be obtained.

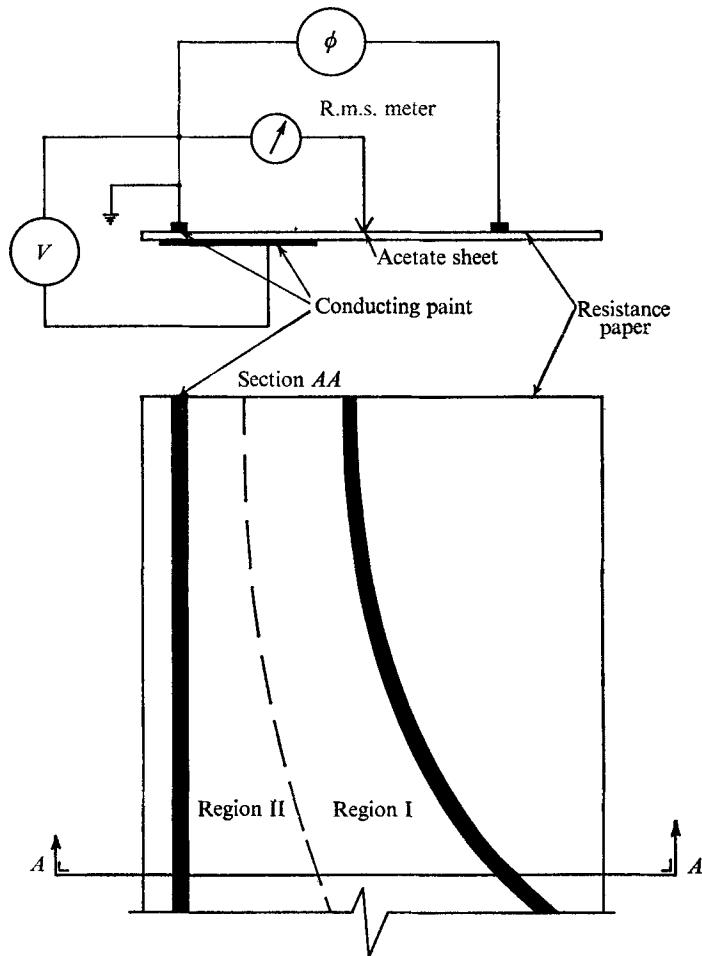The electrical analog is thus able to provide quick and accurate solutions of the

FIGURE 3. Arrangement of electrical analog. $V \gg \phi$.

governing equations. At the present stage of development, the method suffers from the minor limitation that the vorticity must be constant throughout the vortical region.

## 5. Experimental investigation

### 5.1. *Experimental apparatus and boundary-layer control*

All the experimental work was carried out in a low-speed open-return wind tunnel at the University of Melbourne. The working section of this tunnel is of rectangular cross-section $110 \times 610$ mm at the inlet and 2·5 m long with a specially constructed flexible roof, allowing any desired streamwise pressure gradient to be attained. The floor of the working section consists of highly polished plywood (supported on aluminium channels) pressure tapped at 2·5 cm intervals along its centre-line.

The shape of the flexible roof was adjusted to obtain an adverse-pressure-gradient boundary layer upstream of the desired position of separation. The roof
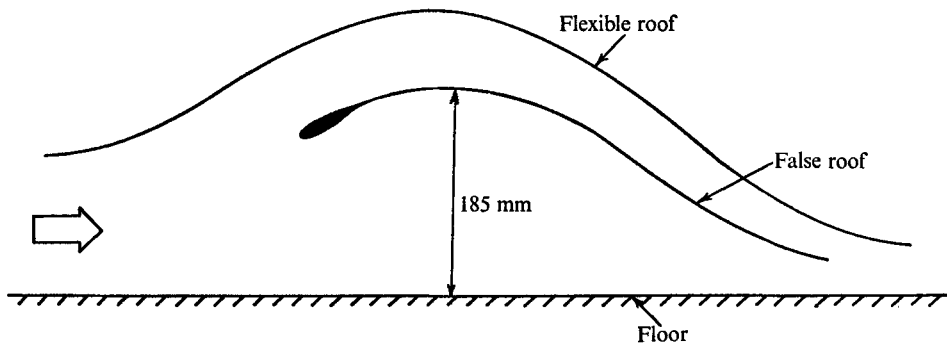
FIGURE 4. Arrangement of false roof. Duct width = 610 mm.

then diverged suddenly to produce a definite position for the separation line and subsequently converged to produce reattachment. As was expected the boundary layer on the roof initially separated, that on the floor remaining attached. Several types of boundary-layer control were tried on the roof but with only moderate success; the floor layer, although separating, showed marked three-dimensionality. After many fruitless attempts the arrangement shown in figure 4 was found to produce an acceptably two-dimensional separation bubble on the floor. This arrangement consisted of a false roof mounted below the flexible roof which provided a starting point for a new roof boundary layer. The old roof layer was completely removed through the passage between the false and flexible roofs. This passage was arranged to be continuously converging, thus avoiding separation within it. The separation line thus obtained was essentially straight over the majority of the duct width and was symmetrical about its centre-line. It was found that, by varying the position of the trailing edge of the false roof, the size of the separation bubble could be varied while still retaining its approximate two-dimensionality. Distributions of the pressure coefficient for the two cases studied are shown in figures 7 (a) and (b) below.

## 5.2. Experimental procedure

Two separated flows were investigated. The first case provided a large separation bubble, enabling detailed measurements to be undertaken inside the bubble. In the second case no discernible bubble could be found although tuft-probe investigations indicated patches of transitory stall, shown in figure 6 (c). This case was designed to provide a second example against which the separation model could be tested.

Velocity traverses were carried out normal to the plate on the duct centre-line throughout the developing boundary layer and, for the first case, throughout the separation bubble. In regions upstream of separation where flow divergence remained insignificant a flattened total pressure probe was used, static pressure variations through the profiles being found to be negligible. In regions of significant flow divergence a twin hot-wire probe described by Fairlie (1973) was used to obtain mean-velocity and flow-angle profiles. Flow angles were obtained with this probe by traversing a temperature-sensitive wire through the wake of

| $x$ (m) | $C_f'$† | $\pi_c$ | $H$ | $\delta^*$ (mm) | $\Delta$ (mm) | $\xi$ |
|---|---|---|---|---|---|---|
| | | *Case* 1. Reynolds number $= 1{\cdot}25 \times 10^6 \, \mathrm{m}^{-1}$ | | | | |
| 0·150 | 0·0034 | 0·55 | 1·44 | 2·30 | — | — |
| 0·300 | 0·0029 | 0·95 | 1·47 | 3·47 | 18·8 | 0·53 |
| 0·450 | 0·0025 | 1·25 | 1·51 | 4·67 | 23·1 | 0·58 |
| 0·600 | 0·0021 | 1·70 | 1·57 | 6·55 | 29·8 | 0·63 |
| 0·750 | 0·0017 | 2·40 | 1·65 | 9·01 | 38·0 | 0·68 |
| 0·900 | 0·0011 | 4·15 | 1·85 | 13·43 | 48·0 | 0·80 |
| | | *Case* 2. *Reynolds number* $= 1{\cdot}9 \times 10^6 \, \mathrm{m}^{-1}$ | | | | |
| 0·450 | 0·0024 | 1·3 | 1·49 | 3·96 | 19·9 | 0·57 |
| 0·600 | 0·0021 | 1·7 | 1·53 | 5·28 | 24·8 | 0·61 |
| 0·750 | 0·0018 | 2·1 | 1·60 | 7·28 | 31·6 | 0·66 |
| 0·900 | 0·0015 | 3·1 | 1·65 | 9·68 | 40·1 | 0·69 |
| 1·000 | 0·0012 | 3·7 | 1·73 | 13·90 | 53·4 | 0·75 |
| 1·090 | 0·0004 | 10·3 | 2·24 | 22·06 | 63·1 | 1·00 |

† $C_f' =$ local skin-friction coefficient as determined from a 'Clauser chart'.

TABLE 1

an upstream velocity-sensitive wire. In spite of flow reversals and nonlinearities, analysis showed that mean velocities and flow angles could be obtained with reasonable accuracy. Throughout these tests the upstream reference velocity was adjusted to maintain a constant Reynolds number ($1{\cdot}25 \times 10^6 \, \mathrm{m}^{-1}$ for case 1 and $1{\cdot}9 \times 10^6 \, \mathrm{m}^{-1}$ for case 2).

## 6. Data reduction and results

### 6.1. *Mean flow field*

All velocity profiles from the upstream developing boundary layer were tested against the 'law of the wall' and 'law of the wake' in the normal way. See Coles (1956). The good agreement found for both cases confirmed that the upstream layers were typical adverse-pressure-gradient turbulent boundary layers.

Mean-velocity profiles prior to separation may be reconstructed by the reader from the data† given in table 1, which gives the values of the Coles wake factor $\pi_c, \delta^*, H$, etc. The correlation of the data according to the defect-law form mentioned earlier is shown in figure 1 and again good agreement is seen.

From an empirical curve fit profiles of

$$\frac{U_1 - u}{U_s} = 1{\cdot}0 - 0{\cdot}4(y/\Delta)^{\frac{1}{2}} - 0{\cdot}6 \sin\left(\frac{\pi}{2}\frac{y}{\Delta}\right) \tag{11}$$

may also be reconstructed. However, these give no information concerning the thin logarithmic region since in the Perry & Schofield model, skin friction is regarded as an irrelevant parameter for these low skin-friction layers.

† A complete set of experimental data will be made available by the authors on request.
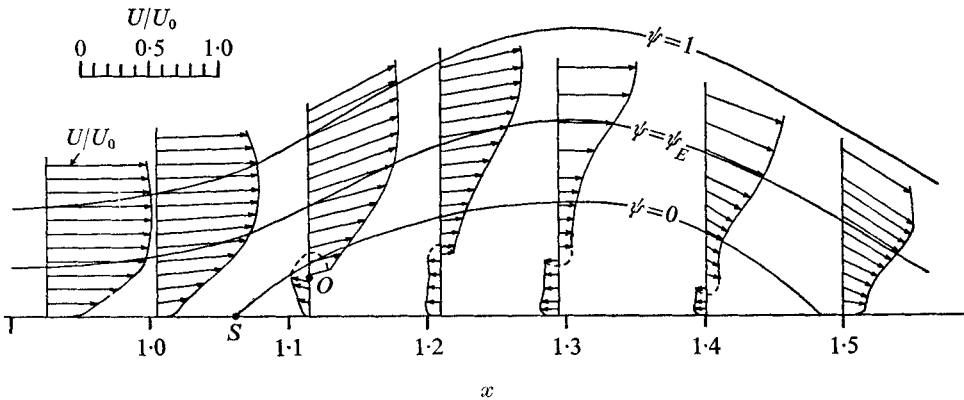
FIGURE 5. Velocity vector field for case 1 obtained from experiment.

The profiles of flow angle and mean velocity through the separated region were expressed in the form

$$\frac{u}{U_0} = \frac{q}{U_0}\cos\beta = f\left(\frac{y}{L}\right), \tag{12}$$

where $q$ is the magnitude and $\beta$ the angle relative to the floor of the mean streamwise velocity at any point. The value of the dimensionless stream function

$$\psi = \int_0^{Y/L} \frac{u}{U_0} d(y/L) \tag{13}$$

was then obtained by numerical integration. The value of $L$ was adjusted such that the streamline coincident with the upper boundary corresponded to the value $\psi = 1$. From a plot of $\psi$ against $y/L$, points of equal $\psi$ and hence streamlines were obtained.

Figure 5 shows the experimental velocity field obtained for case 1. It should be pointed out how difficult it is to calculate the vorticity from such data, particularly close to separation and reattachment. Not only is the component $\partial u/\partial y$ important, but so also is $-\partial v/\partial x$, $v$ being the component of velocity in the $y$ direction. An interesting point about figure 5 is that the velocity profiles in the boundary layer do not develop an inflexion point until an appreciable $v$ component has developed. It can be seen from figure 5 that at about $x = 1\cdot10$ m an appreciable discrepancy develops between the measured flow angles $\beta$ and the streamline directions deduced from (12) and (13). Two possible reasons for this are (a) nonlinear effects in the measuring probe mentioned earlier and (b) three-dimensional effects. The deduced streamline directions were adopted as the correct directions since they appeared to be more consistent with the measured positions of the points $S$ and $O$. Also, in regions where velocities were very low, mean velocities would have been overestimated owing to the presence of large velocity fluctuations. The broken lines shown on the profiles of figure 5 illustrate how the velocity vectors 'bend back' on themselves owing to the changing streamline direction. Flow angles were not measured for case 2 since they were found by cursory checks to be small.

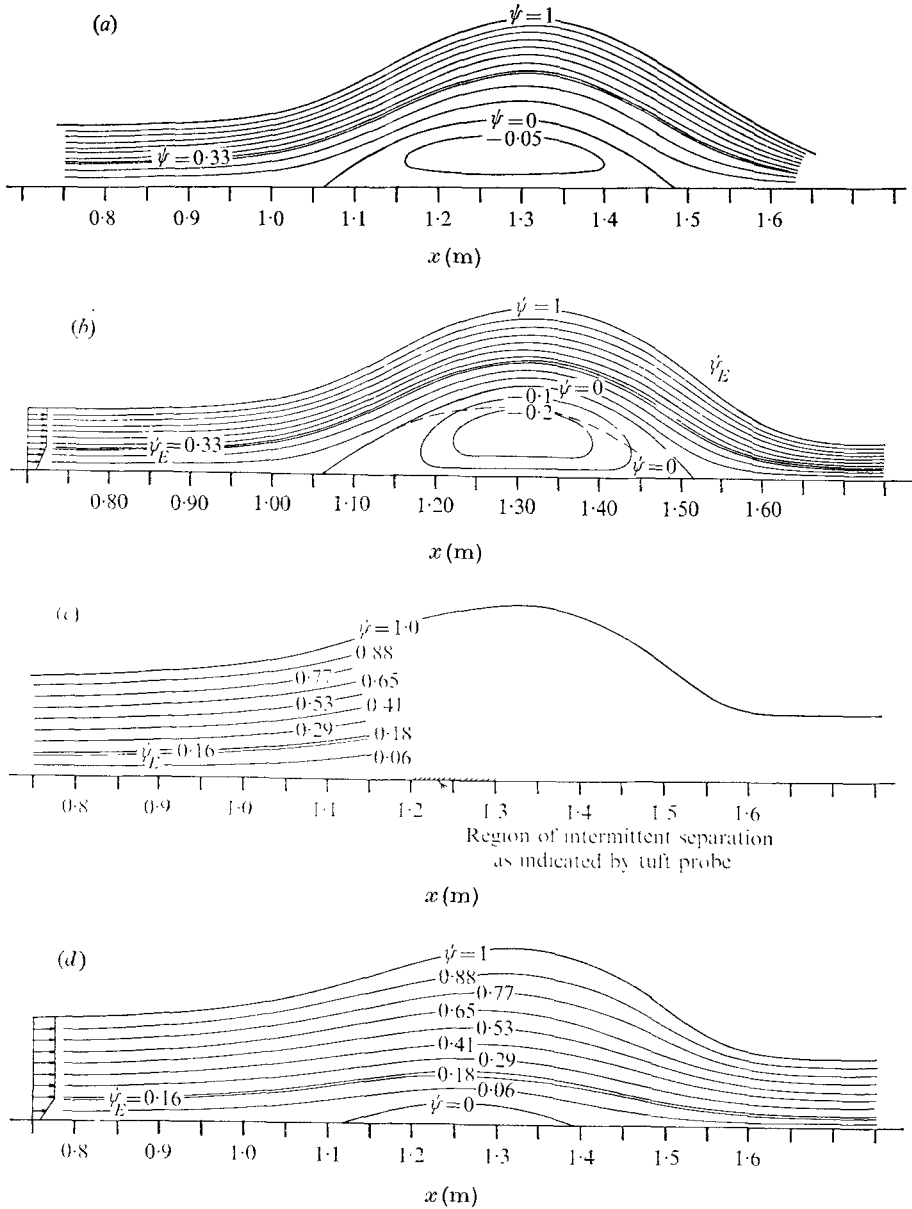The experimental streamline patterns obtained for both cases are shown in

FIGURE 6. Streamline patterns for (a) case 1, experiment; (b) case 1, analog solution;
(c) case 2, experiment; (d) case 2, analog solution.

figures 6 (a) and (c). Velocity profiles were not calculated using the model since it
predicts stream functions. To extract velocities from the model would require
differentiation of the stream function – a very inaccurate process. In any case,
the authors do not feel that the model is sufficiently accurate to calculate detailed
velocity distributions, since the neglect of entrainment and the diffusion of
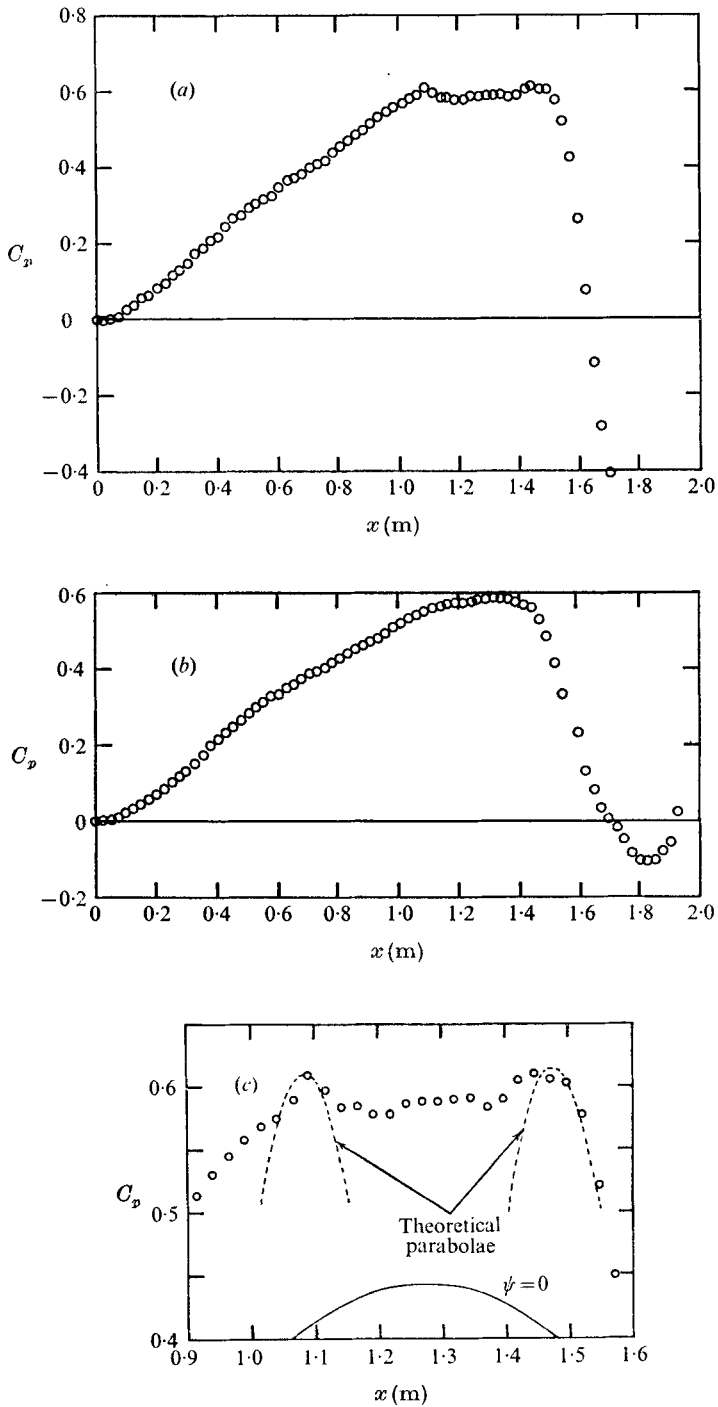vorticity is rather severe. However, as will be seen, the gross features of the flow

FIGURE 7. Surface pressure distributions. (*a*) Case 1. (*b*) Case 2. (*c*) Detail in separated region of case 1 showing osculating parabolae. $C_p = (P - P_{x=0})/\frac{1}{2}\rho(U_1)^2_{x=0}$. (After Perry & Fairlie 1974.)

patterns are predicted reasonably well. In figure 6 (*b*) a comparison between the $\psi = 0$ streamlines and the $\psi = \psi_E$ streamlines from theory and experiment is shown. The close agreement between the $\psi_E$ streamlines shows that the overall displacement effects of the experimental and theoretical bubbles are close.

Perry & Fairlie (1974) have shown that if the constant-vorticity representation is valid for a turbulent boundary layer close to separation then the separation or reattachment angle $\alpha$ will be given by

$$\tan \alpha = \pm\, 2(-P_{xx})^{\frac{1}{2}}/\omega, \tag{14}$$

where $P_{xx}$ is the second derivative of the (kinematic) pressure at the separation or reattachment point. They also found that the pressure will be a maximum at a point of separation or reattachment and hence the pressure distribution will be parabolic in these regions. The detailed pressure distribution in the separated region of case 1 is shown in figure 7 (*c*) and pressure maxima are seen to coincide with the separation and reattachment points. The theoretical parabolic distributions shown were determined from (14) using the separation and reattachment angles measured from the experimental streamline pattern. The value of the vorticity adopted was calculated from the upstream profile. The general agreement found, although not precise, is encouraging considering the inaccuracies involved in $\alpha$ and $\omega$.

Detailed observations of the flow for case 1 were made using tufts, smoke and glass spheres $15\,\mu m$ in diameter as surface flow tracers. (The velocities in the separated region were far too low to allow the use of the usual surface oil flow techniques.) These observations were combined with the mathematical principles proposed by Lighthill (1963) and Oswatitsch (1958) and recently extended by Perry & Fairlie (1974) to produce the surface and 'separation surface' flow patterns shown in figure 8. The flow patterns shown for the wall/floor corners, although consistent mathematically and in agreement with observation, are thought to be somewhat oversimplified. Corner eddies would considerably complicate the small-scale structure.

## 7. Comparisons of model with experiment

The values of $\xi$ and $\Delta$ calculated from the upstream velocity profiles were used to calculate the thickness and vorticity of the vortical layer at the upstream boundary of the model. The location of the upstream boundary was chosen far enough upstream of the separation point to minimize any interaction. This was later checked during the solution of the model equations using the electrical analog. The upper boundary was chosen for the first case to coincide with the experimental streamline which closely approximated the false-roof profile. In the second case, where detailed flow-field measurements did not extend throughout the separated region, the upstream boundary was defined by the false-roof profile and the streamline which appeared to stagnate on the false roof. The solution of the model equations was found to be (relatively) insensitive to the choice of this streamline. The resulting electrical analog solutions for both cases are shown in figure 6 and the model is seen to predict the overall features of the
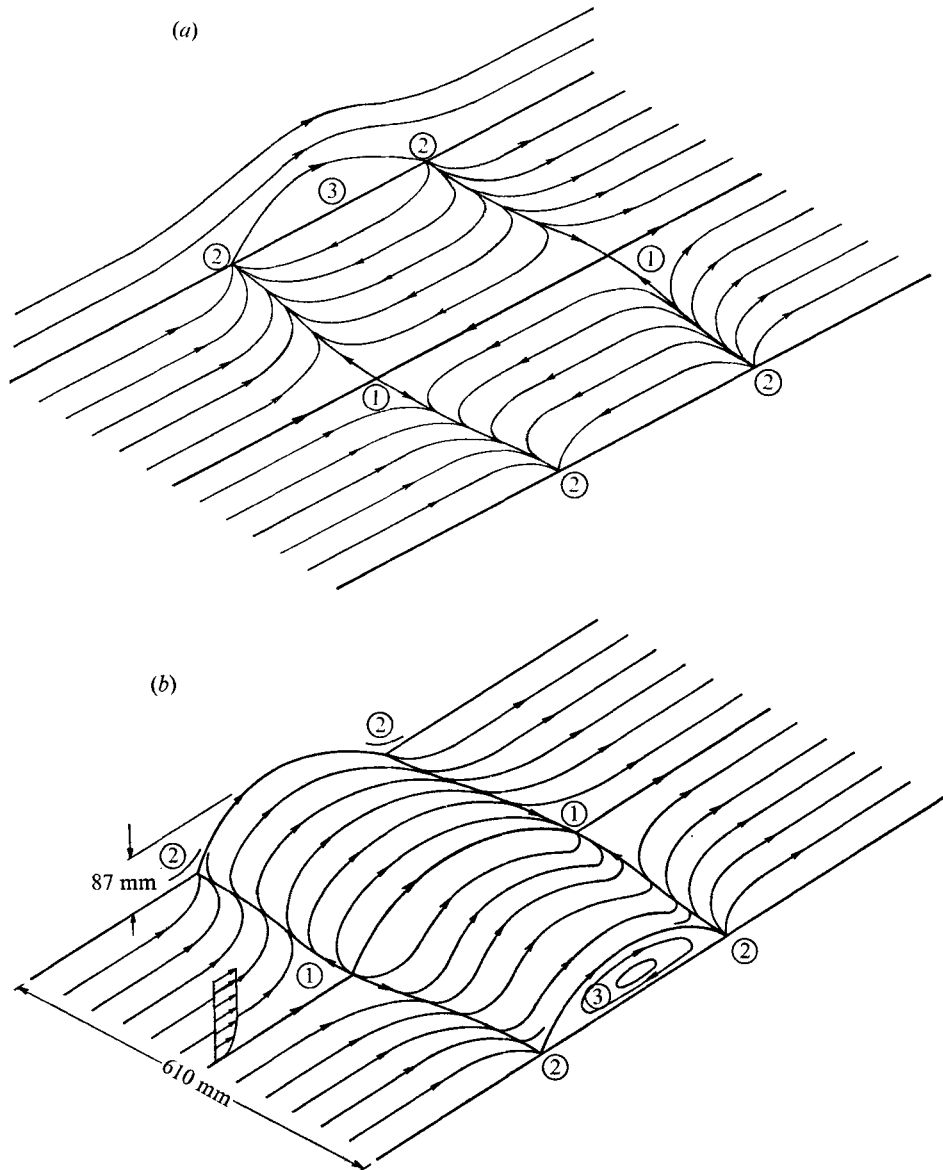
(a)

(b)

87 mm

610 mm

FIGURE 8. Flow patterns for case 1 showing classification of critical points. (a) Surface streamlines. (b) ' Separation surface' streamlines. 1, 'saddle' in plane of floor, ' node' in plane of separation surface; 2, 'node' in plane of floor, ' saddle' in plane of side wall; 3, ' centre' on side wall.

flows reasonably well. In both cases the separation bubble is somewhat larger with the separation point further upstream than is indicated by experiment. Thus, if the model were to be used and in an engineering application, a somewhat conservative result would be obtained. The departures of the model solution from experiment are no doubt due at least in part to the neglect of both entrainment and vorticity diffusion. This will affect the magnitude of the vorticity inside the

separation bubble, which, from a comparison of stream functions in the bubble for case 1 (see figures 6 $a, b$), may be seen to be somewhat less than that in the upstream layer. For more sophisticated models a more detailed study of the mechanisms controlling the value of this vorticity will be required.

## 8. Discussion and conclusions

The inviscid model for turbulent separation has been shown to be capable of predicting the gross properties of the flow fields for two extreme cases (a large bubble and a very small bubble). The authors believe that the model contains the major properties of a turbulent layer which are relevant in the separation process. The model is different from most previous proposals in that the interaction between the boundary layer and the free stream and the elliptic nature of the governing equations are taken into account while the effects of the inner part of the boundary layer and viscosity are assumed to be negligible.

The extension of the model to external flow problems involves the selection of a suitable (known) streamline as an upper boundary. Either this streamline must be far enough from the body to be unaffected by the separation or else some form of iterative process must be adopted. For flows which do not reattach, the extension of the model must await more detailed studies of wake flows to provide knowledge of the appropriate value of the vorticity in the separated region and downstream boundary conditions. This is especially true in the case of the aerofoil problem, for which the present knowledge of the conditions at the trailing edge, where two shear layers interact, and in the ensuing wake is severely limited. However, the application of the model in such cases, making use of empirical assumptions or numerical experimentation, could provide much needed insight into areas which are at present poorly understood.

## REFERENCES

BATCHELOR, G. K. 1956 *J. Fluid Mech.* **1**, 177.

CLAUSER, F. H. 1956 *Adv. in Appl. Mech.* **4**, 1.

COLES, D. E. 1956 *J. Fluid Mech.* **1**, 191.

COLES, D. E. & HIRST, E. A. 1968 *Proc. AFOSR-IFP-Stanford Conf. on Computation of Turbulent Boundary Layers*, vol. 2, p. 55.

FAIRLIE, B. D. 1973 Ph.D. thesis, University of Melbourne.

KLINE, S. J., MORKOVIN, M. V., SOVRAN, G. & COCKRELL, D. J. 1968 *Proc. AFOSR-IFP-Stanford Conf. on Computation of Turbulent Boundary Layers*, vol. 1, p. 464.

KUCHEMANN, D. 1967 *Z. Flugwiss.* **15**, 292.

LIGHTHILL, M. J. 1963 *Laminar Boundary Layers* (ed. L. Rosenhead), p. 46. Oxford University Press.

OSWATITSCH, K. 1958 In *Grenzschichtforshung* (ed. H. Goertler), p. 299. Springer.

PERRY, A. E. & FAIRLIE, B. D. 1974 *Adv. in Geophys.* B **18**, 299.

PERRY, A. E. & SCHOFIELD, W. H. 1973 *Phys. Fluids*, **16**, 2068.

SANDBORN, V. A. 1959 *N.A.S.A. Memo.* no. 2-5-59E.

SMITH, P. D. 1970 *R.A.E. Tech. Memo.* Aero 1217.

STRATFORD, B. S. 1959 *J. Fluid Mech.* **5**, 1.

SWANNELL, J. H. 1963 *Exp. Mech.* **3**, 279.

TAULBEE, D. B. & ROBERTSON, J. M. 1972 *J. Basic Engng, Trans. A.S.M.E.* D **94**, 544.

TOWNSEND, A. A. 1960 *J. Fluid Mech.* **8**, 143.